

Study of the Hadronic Photon Structure Function F_2^γ at LEP

The L3 Collaboration

Abstract

The hadronic photon structure function F_2^γ is studied in the reaction $e^+e^- \rightarrow e^+e^-$ hadrons at LEP with the L3 detector. The data, collected from 1991 to 1995 at a centre-of-mass energy $\sqrt{s} \simeq 91$ GeV, correspond to an integrated luminosity of 140 pb^{-1} . The photon structure function F_2^γ is measured in the Q^2 interval $1.2 \text{ GeV}^2 \leq Q^2 \leq 9.0 \text{ GeV}^2$ and the x interval $0.002 < x < 0.2$. F_2^γ shows a linear growth with $\ln Q^2$. The value of the slope $\alpha^{-1} dF_2^\gamma(Q^2)/d \ln Q^2$ is measured to be $0.079 \pm 0.011 \pm 0.009$.

Submitted to *Phys. Lett. B*

1 Introduction

The photon structure function is measured at e^+e^- storage rings via the interaction of two virtual photons $e^+e^- \rightarrow e^+e^-\gamma^*\gamma \rightarrow e^+e^-$ hadrons (Fig. 1) [1,2]. Here we present the results obtained at LEP with the L3 detector at $\sqrt{s} \simeq 91$ GeV for an integrated luminosity of $\mathcal{L} = 140 \text{ pb}^{-1}$ from 1991 to 1995. A scattered electron is measured in the momentum transfer range $1.2 \text{ GeV}^2 \leq Q^2 \leq 9 \text{ GeV}^2$. The photon (γ^*) of high virtuality is used as a probe for the structure of the quasi-real target photon (γ) with virtuality $t^2 \sim 0$. In analogy with ep deep inelastic scattering (DIS), the cross-section is written as [3]:

$$\frac{d^3\sigma}{dx dQ^2 dx_2} = \frac{2\pi\alpha^2}{xQ^4} \frac{dn(x_2)}{dx_2} [(1 + (1-y)^2)F_2^\gamma(x, Q^2) - y^2 F_L^\gamma(x, Q^2)] \quad (1)$$

where α is the fine structure constant, x_2 is the energy of the target photon relative to the beam energy, F_2^γ and F_L^γ are photon structure functions. The flux of the quasi-real target photons $dn(x_2)/dx_2$ is calculated by the Equivalent Photon Approximation (EPA) [3]. The dimensionless deep inelastic scattering variables, x and y , are defined as:

$$x = \frac{Q^2}{Q^2 + t^2 + W_{\gamma\gamma}^2}, \quad y = 1 - \frac{E_{tag}}{E_{beam}} \cos^2 \frac{\theta_{tag}}{2} \quad (2)$$

where E_{beam} is the beam energy, E_{tag} and θ_{tag} are the energy and polar angle of the measured electron¹⁾ and $W_{\gamma\gamma}$ is the mass of the two-photon state. In the kinematic regime studied here ($E_{tag} \sim E_{beam}$), y is so small ($\langle y \rangle \sim 0.08$) that the measured cross-section is only sensitive to the structure function F_2^γ . We study the structure function in the low x region $0.002 < x < 0.2$.

Several types of physical processes contribute to F_2^γ . A point-like coupling of the photons to a quark-antiquark pair (Quark Parton Model, QPM) gives a contribution that is calculable in QED in the same way as for the process $e^+e^- \rightarrow e^+e^-l^+l^-$ which we studied previously [4]. The photon may also fluctuate into a virtual vector meson via a non-perturbative effective coupling. The partonic constituents of the vector meson may be probed by the highly virtual photon (Vector Dominance Model, VDM). Finally, the virtual partonic content of the target photon, quarks or gluons, may participate in a hard scattering process, leading to the so called ‘‘resolved photon’’ contribution.

The point-like part of F_2^γ is peaked at large x , whereas at small x the gluon radiation of quarks gives the dominant contribution. Perturbative QCD predicts the evolution of F_2^γ as a function of $\ln Q^2$, but the quark and gluon distributions inside the photon must be determined experimentally. Since the uncertainty of the present measurements is large, there exist several models with rather different predictions for the small x behaviour. We compare our data to the GRV-LO [5] parametrisation where the Q^2 evolution starts at $Q_0^2 = 0.25 \text{ GeV}^2$, SaS-1d [6] with $Q_0^2 = 0.36 \text{ GeV}^2$ and LAC [7] with $Q_0^2 = 4 \text{ GeV}^2$. In the LAC model we consider two versions, LAC1 and LAC2. In the SaS-1d model the effect of non-zero target photon virtuality is also taken into account.

2 Monte Carlo models

Three different Monte Carlo generators are used in this study: PHOJET [8], HERWIG [9] and TWOGAM [10].

¹⁾Electron stands for electron or positron throughout this paper.

PHOJET is an event generator for pp, γp and $\gamma\gamma$ interactions, described within the Dual Parton Model (DPM). It gives a good description of the events $\gamma\gamma \rightarrow$ hadrons that we studied at $Q^2 \simeq 0$ [11]. A transverse momentum cutoff, $p_t^{cut} = 2.5$ GeV, is applied to the partons of the resolved photons to separate soft from hard processes [12]. The complete lepton-photon vertex for transversely polarised photons is simulated in the program.

HERWIG is a general-purpose QCD Monte Carlo generator to simulate hadron emission reactions with interfering gluons. The high Q^2 events are described as a DIS process, $e\gamma \rightarrow e +$ hadrons, including the full kinematics of the scattering electron. The flux of target photons is generated using the EPA [3].

TWOGAM generates three different processes separately: the Quark Parton Model, the Vector Dominance Model and the QCD resolved photon contribution. The VDM part is generated according to Ref. [13]:

$$\sigma_{\gamma\gamma}(W_{\gamma\gamma}, Q^2, t^2) = \sum_{i=T,S} F_i(Q^2) \cdot F_i(t^2) \cdot \sigma_{\gamma\gamma}(W_{\gamma\gamma}) \quad (3)$$

where T (transverse) and S (scalar) are the polarisation indices of the virtual photons. The generalized VDM (GVDM) form factor [14] F_i describes the Q^2 and t^2 dependences. For $\sigma_{\gamma\gamma}(W_{\gamma\gamma})$, we use our total cross-section measurement [11]. As in PHOJET a cutoff, $p_t^{cut} = 2.3$ GeV, is applied to separate soft and hard processes.

The dominant background sources to the reaction $e^+e^- \rightarrow e^+e^-$ hadrons are $e^+e^- \rightarrow e^+e^-\tau^+\tau^-$, simulated by the program of Vermaseren et al. [15], and $e^+e^- \rightarrow$ hadrons, simulated by JETSET [16]. The background from $e^+e^- \rightarrow \tau^+\tau^-$ is simulated by KORALZ [17].

All Monte Carlo events are passed through a full detector simulation using the GEANT [18] and the GEISHA [19] programs and they are reconstructed in the same way as the data.

3 Data Analysis

3.1 Event Selection

A detailed description of the L3 detector is given in Ref. [20]. The single tagged two-photon hadronic events are triggered by the central track trigger (84% of events with an efficiency of 81%) and by the single tag trigger (81% of events with an efficiency of 76%). The central track trigger [21] requires at least two charged particles, each with $p_t > 150$ MeV, back-to-back in the transverse plane within 41° . The single tag trigger [22] requires at least 30 GeV deposited in one of the small angle electromagnetic calorimeters, in coincidence with at least one track in the central tracking chamber. The total trigger efficiency is $95 \pm 3\%$ which takes into account also the high level software triggers [23] and is almost independent of the visible mass of the hadronic final state.

Candidate single tagged two-photon hadronic events are selected by the following cuts:

- A tagged electron is identified as the highest energy cluster in one of the small angle electromagnetic calorimeters with $E_{tag} > 35$ GeV and a polar angle in the range $26 \text{ mrad} < \theta_{tag} < 66 \text{ mrad}$.
- The energy of the most energetic cluster in the small angle electromagnetic calorimeter opposite to the identified tagged electron is required to be less than 12 GeV (anti-tag condition).

- The number of charged particles must be greater than two. The charged particles are selected by requiring a transverse momentum, p_t , larger than 100 MeV and a distance of closest approach in the transverse plane to the interaction vertex smaller than 10 mm.
- The visible invariant mass, W_{vis} , of the hadronic final state, calculated from the tracks and the calorimetric clusters, is required to be in the range $3 \text{ GeV} \leq W_{vis} \leq 40 \text{ GeV}$. The energy clusters in the small angle electromagnetic calorimeter, excluding the tagged electron, are assumed to be pions and are also included in the W_{vis} calculation.
- The transverse momentum component of the hadronic state perpendicular to the tag plane, p_t^{out} , is required to be less than 5 GeV. The tag plane is defined by the beam axis and the tagged electron. The sum of the transverse momentum of the tagged electron and the transverse momentum component of the hadronic state in the tag plane, p_t^{bal} , has to be smaller than 5 GeV.

After the selection cuts, a total of 9928 events is selected in the Q^2 range $1.2 \text{ GeV}^2 \leq Q^2 \leq 9 \text{ GeV}^2$. The sample is divided into two Q^2 bins of similar statistics: $1.2 \text{ GeV}^2 \leq Q^2 < 3 \text{ GeV}^2$ and $3 \text{ GeV}^2 \leq Q^2 \leq 9 \text{ GeV}^2$. Table 1 shows the number of selected events and the expected backgrounds from $e^+e^- \rightarrow e^+e^-\tau^+\tau^-$ and $e^+e^- \rightarrow \text{hadrons}$. The background contamination is small. The contamination of $e^+e^- \rightarrow \tau^+\tau^-$ is negligible. The contamination from beam gas and beam wall events is found to be negligible by inspection of the radial distribution of track intersections and considering the ratio of the number of positive and negative charged particles.

To improve the measurement of W_{vis} , we include the kinematics of the tagged electron in the visible mass calculation. Assuming that the transverse momentum of the target photon is negligible, we define W_{rec} , as suggested in Ref. [24]:

$$W_{rec}^2 \equiv (p_+^{e_{in}} - p_+^{e_{tag}}) \left(\sum_i p_-^i \right) - |p_t^{e_{tag}}|^2 \quad (4)$$

where i runs over all measured hadrons, e_{in} is the initial particle, e_{tag} the tagged electron and $p_{\pm} \equiv E \pm p_z$. The comparison of $W_{\gamma\gamma}$, W_{vis} and W_{rec} is shown in Fig. 2. A significant improvement is seen in the W_{rec} variable which uses the constraint of transverse momentum conservation.

3.2 Comparison of data and Monte Carlo

Due to the finite detector resolution and acceptance, the correlation of W_{rec} and $W_{\gamma\gamma}$ depends on the modelling of the final state. Therefore a good modelling is necessary for an accurate measurement of F_2^{γ} . To choose the best model we have compared single particle and global event distributions of the data to Monte Carlo predictions.

As an example the W_{rec} and Q^2 spectra are shown in Fig. 3a and 3b. All three Monte Carlos give a reasonable description of the data. The x_{vis} and x_{rec} spectra, calculated by Eq. 2 with W_{vis} and W_{rec} , respectively, are rather well reproduced by PHOJET and TWOGAM (Fig. 3c and 3d). HERWIG disagrees with the data in the small x region. The comparison in the p_t spectrum of charged particles is shown in Fig. 4. HERWIG disagrees with the data in the high p_t region. The energy flow versus the pseudorapidity, defined as $\eta = -\ln(\tan(\theta/2))$ where θ is the polar angle of final state particles, is shown in different Q^2 and x_{rec} ranges in Fig. 5. The tag direction is always on the negative side and the energy of the tagged electron is not shown in the plot. Reasonable agreement between data and the different Monte Carlo predictions is

found for the large x_{rec} values. At small values of x_{rec} , both TWOGAM and HERWIG deposit too much energy in the forward region but TWOGAM reproduces better the data in the central region.

From a statistical comparison of many distributions [25] we see that PHOJET shows the overall best agreement with the data. TWOGAM reproduces our data better with $p_t^{cut} = 2.3$ GeV than with the default value $p_t^{cut} = 1.8$ GeV [10]. Because of the large discrepancies with the data, we do not use HERWIG for the results.

3.3 Unfolding and Extraction of F_2^γ

As shown in Fig. 2, the observed W_{rec} is smaller than the true two-photon invariant mass $W_{\gamma\gamma}$. Therefore the value of x_{rec} is larger than the true value of x . To extract the x distribution, the same unfolding technique [26] is used as in Ref. [11]:

$$x(i) = \sum_j A_{ij} x_{rec}(j) \quad , \quad A_{ij} = \frac{P(x_{rec}(j)|x(i))P(x(i))}{\sum_l P(X_{rec}(j)|x(l))P(x(l))} \quad (5)$$

where $P(x_{rec}|x)$ is the likelihood of measuring x_{rec} given a generated x value and $P(x)$ is the generated x distribution after detector acceptance cuts. The matrix A_{ij} is obtained from the Monte Carlo. After unfolding, the differential cross section in each x interval is calculated by correcting for detector acceptance.

Neglecting the y^2 term in Eq. 1, the differential cross-section is proportional to the structure function F_2^γ :

$$F_2^\gamma(x, Q^2) = \frac{1}{K(x, Q^2)} \times \frac{d^2\sigma}{dx dQ^2} \quad (6)$$

The average weight, $K(x, Q^2)$, for each bin of x and Q^2 is calculated semi-analytically as described in detail in Ref. [4].

3.4 x dependence of F_2^γ

The data are subdivided in six x bins for each Q^2 interval ($1.2 \text{ GeV}^2 \leq Q^2 < 3 \text{ GeV}^2$ and $3 \text{ GeV}^2 \leq Q^2 \leq 9 \text{ GeV}^2$) and unfolded with PHOJET for the variable x_{rec} . The results are given in Table 2.

The uncertainties from the selection procedure are estimated by varying the cuts on E_{tag} , θ_{tag} , number of charged particles, p_t^{out} and p_t^{bal} . The uncertainties from the individual selection cuts are added in quadrature.

The difference of F_2^γ obtained using x_{rec} or x_{vis} measures the unfolding uncertainty; the maximum difference is 10% at the lowest and highest x points. The second error in Table 2 is the quadratic sum of the uncertainties from the selection and unfolding. To study the modelling dependence of the measured F_2^γ , we compare the data corrected with PHOJET and with TWOGAM (Table 2). The difference at large x (maximum 14%) is smaller than the one at low x (maximum 28%).

Radiative corrections are checked by using the Monte Carlo program RADCOR [27], which includes real and virtual photon radiation from the incoming and outgoing electrons to first order in α . The effect on F_2^γ is estimated to be 1 to 2%. Compared to the measurement uncertainties, this correction can be neglected.

The mean value of the virtuality of the target photon, $\langle t^2 \rangle$, is about 0.075 GeV², as estimated by PHOJET and TWOGAM, or 0.087 GeV², as estimated by the QPM as implemented in TWOGAM. The change of F_2^γ because of a non-zero $\langle t^2 \rangle$ is estimated by two different models: SaS-1d [6] and GVDM [14]. For the GVDM model, the value of F_2^γ decreases by 7.5% with a slight x dependence ($\sim 1\%$ in the studied x range). For the parametrisation of SaS-1d, F_2^γ decreases by 10 to 20% depending on the x value. Since the non-zero $\langle t^2 \rangle$ effect depends upon the unknown mixture of point-like and hadronic photon coupling in the data, we do not apply any correction for it. For example, the simulation of TWOGAM gives a mixture of 34% QPM, 54% VDM and 12% QCD in our kinematic range.

The measured values of F_2^γ in two different Q^2 bins are shown in Fig. 6. The predictions for $t^2 = 0$ of GRV-LO, LAC and SaS-1d are superimposed on the data. For SaS-1d, the $t^2 \neq 0$ effect is also shown. The predictions of GRV-LO and SaS-1d lie below the measured F_2^γ values. The LAC model, with $Q_0^2 = 4$ GeV², is apparently consistent with our data at $\langle Q^2 \rangle = 5$ GeV² but it has too steep a Q^2 dependence as shown below.

3.5 Q^2 evolution of F_2^γ

To study the Q^2 evolution of F_2^γ , the data are unfolded in four Q^2 bins in the x interval $0.01 < x < 0.1$. The result is shown in Table 3 and in Fig. 7. The function $a + b \ln Q^2$ is fitted to the data taking into account the statistical and systematic errors from the data selection and unfolding. The fit result is:

$$F_2^\gamma(Q^2)/\alpha = (0.131 \pm 0.012 \pm 0.021) + (0.079 \pm 0.011 \pm 0.009) \times \ln(Q^2/\text{GeV}^2)$$

$$\chi^2/dof = 2.52/2$$

The correlation coefficient between the two parameters is -0.93 . The second error on the coefficients gives the uncertainties from the Monte Carlo models, estimated by repeating the fit with values unfolded from TWOGAM.

The measured F_2^γ shows clearly a linear growth with $\ln Q^2$ as expected. The fitted value of slope b is similar to the value $0.10 \pm 0.02_{-0.02}^{+0.05}$ obtained by OPAL [2] in the adjacent interval $0.1 < x < 0.6$. The predictions of the GRV-LO, LAC and SaS-1d models are also shown in Fig. 7. The GRV-LO agrees reasonably well with the data. The slope predicted by LAC is much larger than our fitted value. The slope predictions of SaS-1d are too low compared to the data.

4 Conclusions

The photon structure function F_2^γ has been measured at LEP with the L3 detector at $\sqrt{s} \simeq 91$ GeV. The measurement is done in the Q^2 interval from 1.2 to 9.0 GeV². The x range is $0.002 < x < 0.1$ for $\langle Q^2 \rangle = 1.9$ GeV² and $0.005 < x < 0.2$ for $\langle Q^2 \rangle = 5.0$ GeV².

At low values of x the data are above the predictions of the GRV-LO and SaS-1d models, indicating a higher contribution of gluons in the photon structure function. The LAC model can reproduce the x behaviour of F_2^γ at $\langle Q^2 \rangle = 5$ GeV² but it predicts too fast a rise of F_2^γ as a function of $\ln Q^2$. In the interval $0.01 < x < 0.1$ the value of F_2^γ increases linearly as a function of $\ln Q^2$, with a slope $\alpha^{-1} dF_2^\gamma(Q^2)/d \ln Q^2 = 0.079 \pm 0.011 \pm 0.009$.

Acknowledgements

We express our gratitude to the CERN accelerator divisions for the excellent performance of the LEP machine. We acknowledge with appreciation the effort of all engineers, technicians and support staff who have participated in the construction and maintenance of this experiment.

The L3 Collaboration:

M. Acciarri,²⁷ O. Adriani,¹⁶ M. Aguilar-Benitez,²⁶ S. Ahlen,¹¹ J. Alcaraz,²⁶ G. Alemani,²² J. Allaby,¹⁷ A. Aloisio,²⁹
M.G. Alvigi,²⁹ G. Ambrosi,¹⁹ H. Anderhub,⁴⁸ V.P. Andreev,³⁷ T. Angelescu,¹³ F. Anselmo,⁹ A. Arefiev,²⁸ T. Azemoon,³
T. Aziz,¹⁰ P. Bagnaia,³⁶ L. Baksay,⁴³ R.C. Ball,³ S. Banerjee,¹⁰ Sw. Banerjee,¹⁰ K. Banicz,⁴⁵ A. Barczyk,^{48,46} R. Barillère,¹⁷
L. Barone,³⁶ P. Bartalini,²² A. Baschirotto,²⁷ M. Basile,⁹ R. Battiston,³³ A. Bay,²² F. Becattini,¹⁶ U. Becker,¹⁵ F. Behner,⁴⁸
J. Berdugo,²⁶ P. Berges,¹⁵ B. Bertucci,³³ B.L. Betev,⁴⁸ S. Bhattacharya,¹⁰ M. Biasini,³³ A. Biland,⁴⁸ G.M. Bilei,³³
J.J. Blaising,⁴ S.C. Blyth,³⁴ G.J. Bobbink,² R. Bock,¹ A. Böhm,¹ L. Boldizar,¹⁴ B. Borgia,^{17,36} D. Bourilkov,⁴⁸
M. Bourquin,¹⁹ D. Boutigny,⁴ S. Braccini,¹⁹ J.G. Branson,³⁹ V. Brigljevic,⁴⁸ I.C. Brock,³⁴ A. Buffini,¹⁶ A. Buijs,⁴⁴
J.D. Burger,¹⁵ W.J. Burger,³³ J. Busenitz,⁴³ X.D. Cai,¹⁵ M. Campanelli,⁴⁸ M. Capell,¹⁵ G. Cara Romeo,⁹ G. Carlino,²⁹
A.M. Cartacci,¹⁶ J. Casaus,²⁶ G. Castellini,¹⁶ F. Cavallari,³⁶ N. Cavallo,²⁹ C. Cecchi,¹⁹ M. Cerrada,²⁶ F. Cesaroni,²³
M. Chamizo,²⁶ Y.H. Chang,⁵⁰ U.K. Chaturvedi,¹⁸ M. Chemarin,²⁵ A. Chen,⁵⁰ G. Chen,⁷ G.M. Chen,⁷ H.F. Chen,²⁰
H.S. Chen,⁷ M. Chen,¹⁵ G. Chiefari,²⁹ C.Y. Chien,⁵ L. Cifarelli,³⁸ F. Cindolo,⁹ C. Civinini,¹⁶ I. Clare,¹⁵ R. Clare,¹⁵
G. Coignet,⁴ A.P. Colijn,² N. Colino,²⁶ S. Costantini,⁸ F. Cotorobai,¹³ B. de la Cruz,²⁶ A. Csilling,¹⁴ T.S. Dai,¹⁵
R.D' Alessandri,¹⁶ R. de Asmundis,²⁹ A. Degre,⁴ K. Deiters,⁴⁶ P. Denes,³⁵ F. DeNotaristefani,³⁶ M. Diemoz,³⁶
D. van Dierendonck,² F. Di Lodovico,⁴⁸ C. Dionisi,^{17,36} M. Dittmar,⁴⁸ A. Dominguez,³⁹ A. Doria,²⁹ M.T. Dova,^{18,4}
E. Drago,²⁹ D. Duchesneau,⁴ P. Duinker,² I. Duran,⁴⁰ S. Easo,³³ H. El Mamouni,²⁵ A. Engler,³⁴ F.J. Eppling,¹⁵ F.C. Erne,²
J.P. Ernenwein,²⁵ P. Extermann,¹⁹ M. Fabre,⁴⁶ R. Faccini,³⁶ M.A. Falagan,²⁶ S. Falciano,³⁶ A. Favara,¹⁶ J. Fay,²⁵ O. Fedin,³⁷
M. Felcini,⁴⁸ T. Ferguson,³⁴ F. Ferroni,³⁶ H. Fesefeldt,¹ E. Fiandrini,³³ J.H. Field,¹⁹ F. Filthaut,¹⁷ P.H. Fisher,¹⁵ I. Fisk,³⁹
G. Forconi,¹⁵ L. Fredj,¹⁹ K. Freudenreich,⁴⁸ C. Furetta,²⁷ Yu. Galaktionov,^{28,15} S.N. Ganguli,¹⁰ P. Garcia-Abia,⁶
M. Gataullin,³² S.S. Gau,¹² S. Gentile,³⁶ J. Gerald,⁵ N. Gheordanescu,¹³ S. Giagu,³⁶ S. Goldfarb,²² J. Goldstein,¹¹
Z.F. Gong,²⁰ A. Gougas,⁵ G. Gratta,³² M.W. Gruenewald,⁸ R. van Gulik,² V.K. Gupta,³⁵ A. Gurtu,¹⁰ L.J. Gutay,⁴⁵
D. Haas,⁶ B. Hartmann,¹ A. Hasan,³⁰ D. Hatzifotiadou,⁹ T. Hebbeker,⁸ A. Herve,¹⁷ P. Hidas,¹⁴ J. Hirschfelder,³⁴
W.C. van Hoek,³¹ H. Hofer,⁴⁸ H. Hoorani,³⁴ S.R. Hou,⁵⁰ G. Hu,⁵ I. Iashvili,⁴⁷ B.N. Jin,⁷ L.W. Jones,³ P. de Jong,¹⁷
L. Josa-Mutuberria,²⁶ A. Kasser,²² R.A. Khan,¹⁸ D. Kamrad,⁴⁷ J.S. Kapustinsky,²⁴ Y. Karyotakis,⁴ M. Kaur,^{18,4}
M.N. Kienzle-Focacci,¹⁹ D. Kim,³⁶ D.H. Kim,⁴² J.K. Kim,⁴² S.C. Kim,⁴² W.W. Kinnison,²⁴ A. Kirkby,³² D. Kirkby,³²
J. Kirkby,¹⁷ D. Kiss,¹⁴ W. Kittel,³¹ A. Klimentov,^{15,28} A.C. König,³¹ A. Kopp,⁴⁷ I. Korolko,²⁸ V. Koutsenko,^{15,28}
R.W. Kraemer,³⁴ W. Krenz,¹ A. Kunin,^{15,28} P. Lacentre,^{47,44} P. Ladron de Guevara,²⁶ G. Landi,¹⁶ C. Lapoint,¹⁵
K. Lassila-Perini,⁴⁸ P. Laurikainen,²¹ A. Lavorato,³⁸ M. Lebeau,¹⁷ A. Lebedev,¹⁵ P. Lebrun,²⁵ P. Lecomte,⁴⁸ P. Lecoq,¹⁷
P. Le Coultre,⁴⁸ H.J. Lee,⁸ C. Leggett,³ J.M. Le Goff,¹⁷ R. Leiste,⁴⁷ E. Leonardi,³⁶ P. Levchenko,³⁷ C. Li,²⁰ C.H. Lin,⁵⁰
W.T. Lin,⁵⁰ F.L. Linde,^{2,17} L. Lista,²⁹ Z.A. Liu,⁷ W. Lohmann,⁴⁷ E. Longo,³⁶ W. Lu,³² Y.S. Lu,⁷ K. Lübelmeyer,¹
C. Luci,^{17,36} D. Luckey,¹⁵ L. Luminari,³⁶ W. Luster mann,⁴⁸ W.G. Ma,²⁰ M. Maity,¹⁰ G. Majumder,¹⁰ L. Malgeri,¹⁷
A. Malinin,²⁸ C. Mañá,²⁶ D. Mangeol,³¹ P. Marchesini,⁴⁸ G. Marian,^{43,4} A. Marin,¹¹ J.P. Martin,²⁵ F. Marzano,³⁶
G.G.G. Massaro,² K. Mazumdar,¹⁰ S. Mele,¹⁷ L. Merola,²⁹ M. Meschini,¹⁶ W.J. Metzger,³¹ M. von der Mey,¹ Y. Mi,²²
D. Migani,⁹ A. Mihul,³ A.J.W. van Mil,³¹ H. Milcent,¹⁷ G. Mirabelli,³⁶ J. Mnich,¹⁷ P. Molnar,⁸ B. Monteleoni,¹⁶ R. Moore,³
T. Moulík,¹⁰ R. Mount,³² F. Muheim,¹⁹ A.J.M. Muijs,² S. Nahn,¹⁵ M. Napolitano,²⁹ F. Nessi-Tedaldi,⁴⁸ H. Newman,³²
T. Niessen,¹ A. Nippe,²² A. Nisati,³⁶ H. Nowak,⁴⁷ Y.D. Oh,⁴² G. Organtini,³⁶ R. Ostonen,²¹ S. Palit,¹² C. Palomares,²⁶
D. Pandoulas,¹ S. Paoletti,³⁶ P. Paolucci,²⁹ H.K. Park,³⁴ I.H. Park,⁴² G. Pascale,³⁶ G. Passaleva,¹⁷ S. Patricelli,²⁹ T. Paul,¹²
M. Pauluzzi,³³ C. Paus,¹⁷ F. Pauss,⁴⁸ D. Peach,¹⁷ Y.J. Pei,¹ S. Pensotti,²⁷ D. Perret-Gallix,⁴ B. Petersen,³¹ S. Petrak,⁸
A. Pevsner,⁵ D. Piccolo,²⁹ M. Pieri,¹⁶ P.A. Piroué,³⁵ E. Pistolesi,²⁷ V. Plyaskin,²⁸ M. Pohl,⁴⁸ V. Pojidaev,^{28,16} H. Postema,¹⁵
J. Pothier,¹⁷ N. Produit,¹⁹ D. Prokofiev,³⁷ J. Quartieri,³⁸ G. Rahal-Callot,⁴⁸ N. Raja,¹⁰ P.G. Rancoita,²⁷ M. Rattaggi,²⁷
G. Raven,³⁹ P. Razis,³⁰ D. Ren,⁴⁸ M. Rescigno,³⁶ S. Reucroft,¹² T. van Rhee,⁴⁴ S. Riemann,⁴⁷ K. Riles,³ O. Rind,³
A. Robohm,⁴⁸ J. Rodin,⁴³ B.P. Roe,³ L. Romero,²⁶ S. Rosier-Lees,⁴ Ph. Rosselet,²² S. Roth,¹ J.A. Rubio,¹⁷ D. Ruschmeier,⁸
H. Rykaczewski,⁴⁸ J. Salicio,¹⁷ E. Sanchez,²⁶ M.P. Sanders,³¹ M.E. Sarakinos,²¹ G. Sauvage,⁴ C. Schäfer,¹ V. Schegelsky,³⁷
S. Schmidt-Kaerst,¹ D. Schmitz,¹ M. Schneegans,⁴ N. Scholz,⁴⁸ H. Schopper,⁴⁹ D.J. Schotanus,³¹ J. Schwenke,¹
G. Schwering,¹ C. Sciacca,²⁹ D. Sciarino,¹⁹ L. Servoli,³³ S. Shevchenko,³² N. Shivarov,⁴¹ V. Shoutko,²⁸ J. Shukla,²⁴
E. Shumilov,²⁸ A. Shvorob,³² T. Sieden burg,¹ D. Son,⁴² V. Soulimov,²⁹ B. Smith,¹⁵ P. Spillantini,¹⁶ M. Steuer,¹⁵
D.P. Stickland,³⁵ H. Stone,³⁵ B. Stoyanov,⁴¹ A. Straessner,¹ K. Sudhakar,¹⁰ G. Sultanov,¹⁸ L.Z. Sun,²⁰ G.F. Susinno,¹⁹
H. Suter,⁴⁸ J.D. Swain,¹⁸ X.W. Tang,⁷ L. Tauscher,⁶ L. Taylor,¹² C. Timmermans,³¹ Samuel C.C. Ting,¹⁵ S.M. Ting,¹⁵
S.C. Tonwar,¹⁰ J. Tóth,¹⁴ C. Tully,³⁵ K.L. Tung,⁷ Y. Uchida,¹⁵ J. Ulbricht,⁴⁸ E. Valente,³⁶ G. Vesztergombi,¹⁴ I. Vetlitsky,²⁸
G. Viertel,⁴⁸ M. Vivargent,⁴ S. Vlachos,⁶ H. Vogel,³⁴ H. Vogt,⁴⁷ I. Vorobiev,^{17,28} A.A. Vorobyov,³⁷ A. Vorvolakos,³⁰
M. Wadhwa,⁶ W. Wallraff,¹ J.C. Wang,¹⁵ X.L. Wang,²⁰ Z.M. Wang,²⁰ A. Weber,¹ S.X. Wu,¹⁵ S. Wynhoff,¹ J. Xu,¹¹ Z.Z. Xu,²⁰
B.Z. Yang,²⁰ C.G. Yang,⁷ H.J. Yang,⁷ M. Yang,⁷ J.B. Ye,²⁰ S.C. Yeh,⁵¹ J.M. You,³⁴ An. Zalite,³⁷ Yu. Zalite,³⁷ P. Zemp,⁴⁸
Y. Zeng,¹ Z.P. Zhang,²⁰ B. Zhou,¹¹ Y. Zhou,³ G.Y. Zhu,⁷ R.Y. Zhu,³² A. Zichichi,^{9,17,18} F. Ziegler,⁴⁷ G. Zilizi,^{43,4}

- 1 I. Physikalisches Institut, RWTH, D-52056 Aachen, FRG[§]
III. Physikalisches Institut, RWTH, D-52056 Aachen, FRG[§]
 - 2 National Institute for High Energy Physics, NIKHEF, and University of Amsterdam, NL-1009 DB Amsterdam, The Netherlands
 - 3 University of Michigan, Ann Arbor, MI 48109, USA
 - 4 Laboratoire d'Annecy-le-Vieux de Physique des Particules, LAPP, IN2P3-CNRS, BP 110, F-74941 Annecy-le-Vieux CEDEX, France
 - 5 Johns Hopkins University, Baltimore, MD 21218, USA
 - 6 Institute of Physics, University of Basel, CH-4056 Basel, Switzerland
 - 7 Institute of High Energy Physics, IHEP, 100039 Beijing, China[△]
 - 8 Humboldt University, D-10099 Berlin, FRG[§]
 - 9 University of Bologna and INFN-Sezione di Bologna, I-40126 Bologna, Italy
 - 10 Tata Institute of Fundamental Research, Bombay 400 005, India
 - 11 Boston University, Boston, MA 02215, USA
 - 12 Northeastern University, Boston, MA 02115, USA
 - 13 Institute of Atomic Physics and University of Bucharest, R-76900 Bucharest, Romania
 - 14 Central Research Institute for Physics of the Hungarian Academy of Sciences, H-1525 Budapest 114, Hungary[‡]
 - 15 Massachusetts Institute of Technology, Cambridge, MA 02139, USA
 - 16 INFN Sezione di Firenze and University of Florence, I-50125 Florence, Italy
 - 17 European Laboratory for Particle Physics, CERN, CH-1211 Geneva 23, Switzerland
 - 18 World Laboratory, FBLJA Project, CH-1211 Geneva 23, Switzerland
 - 19 University of Geneva, CH-1211 Geneva 4, Switzerland
 - 20 Chinese University of Science and Technology, USTC, Hefei, Anhui 230 029, China[△]
 - 21 SEFT, Research Institute for High Energy Physics, P.O. Box 9, SF-00014 Helsinki, Finland
 - 22 University of Lausanne, CH-1015 Lausanne, Switzerland
 - 23 INFN-Sezione di Lecce and Università Degli Studi di Lecce, I-73100 Lecce, Italy
 - 24 Los Alamos National Laboratory, Los Alamos, NM 87544, USA
 - 25 Institut de Physique Nucléaire de Lyon, IN2P3-CNRS, Université Claude Bernard, F-69622 Villeurbanne, France
 - 26 Centro de Investigaciones Energéticas, Medioambientales y Tecnológicas, CIEMAT, E-28040 Madrid, Spain[‡]
 - 27 INFN-Sezione di Milano, I-20133 Milan, Italy
 - 28 Institute of Theoretical and Experimental Physics, ITEP, Moscow, Russia
 - 29 INFN-Sezione di Napoli and University of Naples, I-80125 Naples, Italy
 - 30 Department of Natural Sciences, University of Cyprus, Nicosia, Cyprus
 - 31 University of Nijmegen and NIKHEF, NL-6525 ED Nijmegen, The Netherlands
 - 32 California Institute of Technology, Pasadena, CA 91125, USA
 - 33 INFN-Sezione di Perugia and Università Degli Studi di Perugia, I-06100 Perugia, Italy
 - 34 Carnegie Mellon University, Pittsburgh, PA 15213, USA
 - 35 Princeton University, Princeton, NJ 08544, USA
 - 36 INFN-Sezione di Roma and University of Rome, "La Sapienza", I-00185 Rome, Italy
 - 37 Nuclear Physics Institute, St. Petersburg, Russia
 - 38 University and INFN, Salerno, I-84100 Salerno, Italy
 - 39 University of California, San Diego, CA 92093, USA
 - 40 Dept. de Física de Partículas Elementales, Univ. de Santiago, E-15706 Santiago de Compostela, Spain
 - 41 Bulgarian Academy of Sciences, Central Lab. of Mechatronics and Instrumentation, BU-1113 Sofia, Bulgaria
 - 42 Center for High Energy Physics, Adv. Inst. of Sciences and Technology, 305-701 Taejeon, Republic of Korea
 - 43 University of Alabama, Tuscaloosa, AL 35486, USA
 - 44 Utrecht University and NIKHEF, NL-3584 CB Utrecht, The Netherlands
 - 45 Purdue University, West Lafayette, IN 47907, USA
 - 46 Paul Scherrer Institut, PSI, CH-5232 Villigen, Switzerland
 - 47 DESY-Institut für Hochenergiephysik, D-15738 Zeuthen, FRG
 - 48 Eidgenössische Technische Hochschule, ETH Zürich, CH-8093 Zürich, Switzerland
 - 49 University of Hamburg, D-22761 Hamburg, FRG
 - 50 National Central University, Chung-Li, Taiwan, China
 - 51 Department of Physics, National Tsing Hua University, Taiwan, China
- [§] Supported by the German Bundesministerium für Bildung, Wissenschaft, Forschung und Technologie
[‡] Supported by the Hungarian OTKA fund under contract numbers T019181, F023259 and T024011.
[¶] Also supported by the Hungarian OTKA fund under contract numbers T22238 and T026178.
[‡] Supported also by the Comisión Interministerial de Ciencia y Tecnología.
[‡] Also supported by CONICET and Universidad Nacional de La Plata, CC 67, 1900 La Plata, Argentina.
[‡] Supported by Deutscher Akademischer Austauschdienst.
[◇] Also supported by Panjab University, Chandigarh-160014, India.
[△] Supported by the National Natural Science Foundation of China.

References

- [1] PLUTO Coll., C. Berger et al., Phys. Lett. B 142 (1984) 111;
TASSO Coll., M. Althoff et al., Z. Phys. C 31 (1986) 527;
TPC/ 2γ Coll., H. Aihara et al., Z. Phys. C 34 (1987) 1;
TOPAZ Coll., K. Muramatsu et al., Phys. Lett. B 332 (1994) 477;
AMY Coll., S.K. Sahu et al., Phys. Lett. B 346 (1995) 208;
DELPHI Coll., P. Abreu et al., Z. Phys. C 69 (1996) 223.
- [2] OPAL Coll., R. Akers et al., Z. Phys. C 61 (1994) 199;
OPAL Coll., K. Ackerstaff et al., Z. Phys. C 74 (1997) 33;
OPAL Coll., K. Ackerstaff et al., Phys. Lett. B 411 (1997) 387;
OPAL Coll., K. Ackerstaff et al., Phys. Lett. B 412 (1997) 225.
- [3] V.M. Budnev et al., Phys. Rep. 15 (1975) 181.
- [4] L3 Coll., M. Acciarri et al., Preprint CERN-EP/98-060, submitted to Phys. Lett. B.
- [5] M. Glück, E. Reya and A. Vogt, Phys. Rev. D 45 (1992) 3986;
M. Glück, E. Reya and A. Vogt, Phys. Rev. D 46 (1992) 1973.
- [6] G.A. Schuler and T. Sjöstrand, Z. Phys. C 68 (1995) 607;
G.A. Schuler and T. Sjöstrand, Phys. Lett. B 376 (1996) 193.
- [7] H. Abramowicz, K. Charchula and A. Levy, Phys. Lett. B 269 (1991) 458.
- [8] PHOJET version 1.05c is used.
R. Engel, Z. Phys. C 66 (1995) 203;
R. Engel and J. Ranft, Phys. Rev. D 54 (1996) 4244.
- [9] HERWIG version 5.9 is used.
G. Marchesini et al., Comp. Phys. Comm. 67 (1992) 465.
- [10] TWOGAM version 1.71 is used.
S. Nova et al., DELPHI Note 90-35 (1990).
We thank our colleagues from DELPHI to make their program available to us.
- [11] L3 Coll., M. Acciarri et al., Phys. Lett. B 408 (1997) 450.
- [12] J.H. Field, F. Kapusta and L. Poggioli, Phys. Lett. B 181 (1986) 362;
J.H. Field, F. Kapusta and L. Poggioli, Z. Phys. C 36 (1987) 121.
- [13] I.F. Ginzburg and V.G. Serbo, Phys. Lett. B 109 (1982) 231.
- [14] J.J. Sakurai and D. Schildknecht, Phys. Lett. B 40 (1972) 121.
- [15] J.A.M. Vermaseren, J. Smith and G. Grammer Jr, Phys. Rev. D 19 (1979) 137;
J.A.M. Vermaseren, Nucl. Phys. B 229 (1983) 347.
- [16] T. Sjöstrand, Comp. Phys. Comm. 82 (1994) 74.
- [17] S. Jadach, Comp. Phys. Comm. 79 (1994) 503.

- [18] R. Brun et al., GEANT 3.15 preprint CERN DD/EE/84-1 (Revised 1987).
- [19] H. Fesefeldt, RWTH Aachen report PITHA 85/2 (1985).
- [20] L3 Coll., B. Adeva et al., Nucl. Inst. Meth. A 289 (1990) 35;
 J.A. Bakken et al., Nucl. Inst. Meth. A 275 (1989) 81;
 O. Adriani et al., Nucl. Inst. Meth. A 302 (1991) 53;
 B. Adeva et al., Nucl. Inst. Meth. A 323 (1992) 109;
 K. Deiters et al., Nucl. Inst. Meth. A 323 (1992) 162;
 M. Chemarin et al., Nucl. Inst. Meth. A 349 (1994) 345;
 M. Acciarri et al., Nucl. Inst. Meth. A 351 (1994) 300;
 G. Basti et al., Nucl. Inst. Meth. A 374 (1996) 293;
 A. Adam et al., Nucl. Inst. Meth. A 383 (1996) 342.
- [21] P. Béné et al., Nucl. Inst. Meth. A 306 (1991) 150.
- [22] R. Bizzarri et al., Nucl. Inst. Meth. A 283 (1989) 799.
- [23] C. Dionisi et al., Nucl. Inst. Meth. A 336 (1993) 78;
 Y. Bertsch et al., Nucl. Inst. Meth. A 340 (1994) 309;
 Y. Bertsch et al., Nucl. Inst. Meth. A 340 (1994) 322.
- [24] L. Lönnblad et al., “ $\gamma\gamma$ event generators”, in Physics at LEP2, ed. G. Altarelli, T. Sjöstrand and F. Zwirner, CERN 96-01 (1996), Volume 2, 201.
- [25] C.H. Lin, L3 Note 2189 (1997)²).
- [26] G. D’Agostini, Nucl. Inst. Meth. A 362 (1996) 489.
- [27] F.A. Berends, P.H. Daverveldt and R. Kleiss, Nucl. Phys. B 253 (1985) 421;
 F.A. Berends, P.H. Daverveldt and R. Kleiss, Comp. Phys. Comm. 40 (1986) 271.

²)This L3 Note is freely available on request from: The L3 secretariat, CERN, CH-1211 Geneva 23, Switzerland. Internet: <http://l3www.cern.ch>

Q^2 (GeV ²)	selected	$e^+e^- \rightarrow e^+e^-\tau^+\tau^-$	$e^+e^- \rightarrow \text{hadrons}$
1.2 - 3.0	5772	117	35
3.0 - 9.0	4156	119	84

Table 1: The number of selected events in data taken at $\sqrt{s} \simeq 91$ GeV, for a total integrated luminosity of 140 pb^{-1} . The expected background contributions from the Monte Carlo simulations [15, 16] are normalised to the data luminosity.

$\langle Q^2 \rangle$ [GeV ²]	x range	$\langle x \rangle$	F_2^γ/α (set1)	F_2^γ/α (set2)
1.9	0.002 - 0.005	0.0035	$0.184 \pm 0.009 \pm 0.013$	$0.231 \pm 0.011 \pm 0.016$
	0.005 - 0.010	0.0075	$0.179 \pm 0.007 \pm 0.009$	$0.199 \pm 0.008 \pm 0.010$
	0.010 - 0.020	0.015	$0.176 \pm 0.006 \pm 0.006$	$0.191 \pm 0.007 \pm 0.006$
	0.020 - 0.030	0.025	$0.191 \pm 0.008 \pm 0.004$	$0.193 \pm 0.008 \pm 0.004$
	0.030 - 0.050	0.040	$0.193 \pm 0.008 \pm 0.007$	$0.199 \pm 0.008 \pm 0.007$
	0.050 - 0.100	0.075	$0.185 \pm 0.007 \pm 0.015$	$0.206 \pm 0.008 \pm 0.017$
5.0	0.005 - 0.010	0.0075	$0.307 \pm 0.021 \pm 0.035$	$0.394 \pm 0.027 \pm 0.045$
	0.010 - 0.020	0.015	$0.282 \pm 0.014 \pm 0.027$	$0.318 \pm 0.016 \pm 0.031$
	0.020 - 0.040	0.030	$0.263 \pm 0.011 \pm 0.015$	$0.277 \pm 0.012 \pm 0.016$
	0.040 - 0.060	0.050	$0.278 \pm 0.013 \pm 0.007$	$0.279 \pm 0.013 \pm 0.007$
	0.060 - 0.100	0.080	$0.270 \pm 0.012 \pm 0.008$	$0.275 \pm 0.012 \pm 0.008$
	0.100 - 0.200	0.150	$0.252 \pm 0.011 \pm 0.029$	$0.287 \pm 0.013 \pm 0.032$

Table 2: The measured F_2^γ/α as a function of x in two Q^2 bins. $\langle Q^2 \rangle$ is the average of Q^2 in the intervals $1.2 \text{ GeV}^2 \leq Q^2 < 3 \text{ GeV}^2$ and $3 \text{ GeV}^2 \leq Q^2 \leq 9 \text{ GeV}^2$. $\langle x \rangle$ is the centre of the x bins. The set1 is unfolded with PHOJET and the set2 unfolded with TWOGAM. The first error is statistical. The second error is the systematic error from the data selection and unfolding.

$\langle Q^2 \rangle$ [GeV ²]	F_2^γ/α (set1)	F_2^γ/α (set2)
1.5	$0.173 \pm 0.004 \pm 0.009$	$0.196 \pm 0.005 \pm 0.010$
2.4	$0.195 \pm 0.005 \pm 0.004$	$0.208 \pm 0.005 \pm 0.004$
3.8	$0.245 \pm 0.006 \pm 0.007$	$0.252 \pm 0.006 \pm 0.007$
6.6	$0.278 \pm 0.009 \pm 0.013$	$0.292 \pm 0.009 \pm 0.014$

Table 3: The measured F_2^γ/α as a function of Q^2 for $0.01 < x < 0.1$. The set1 is unfolded with PHOJET and the set2 unfolded with TWOGAM. The first error is statistical. The second error is the systematic error from the data selection and unfolding.

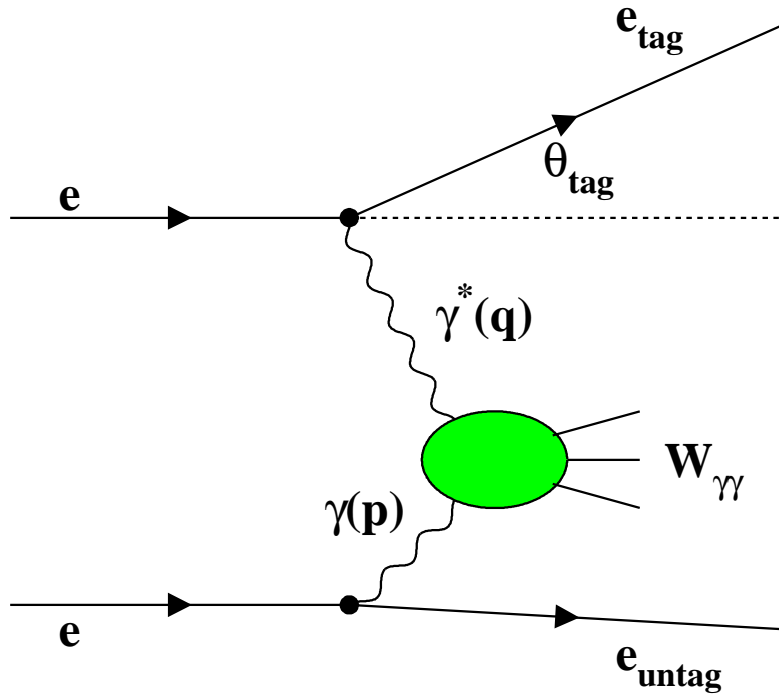


Figure 1: Diagram of a single tagged two-photon interaction $e^+e^- \rightarrow e^+e^-$ hadrons. $W_{\gamma\gamma}$ is the two-photon centre-of-mass energy or the effective mass of the hadronic system. $Q^2 = -q^2$ and $t^2 = -p^2$ are the virtualities of the probe and target photons, respectively.

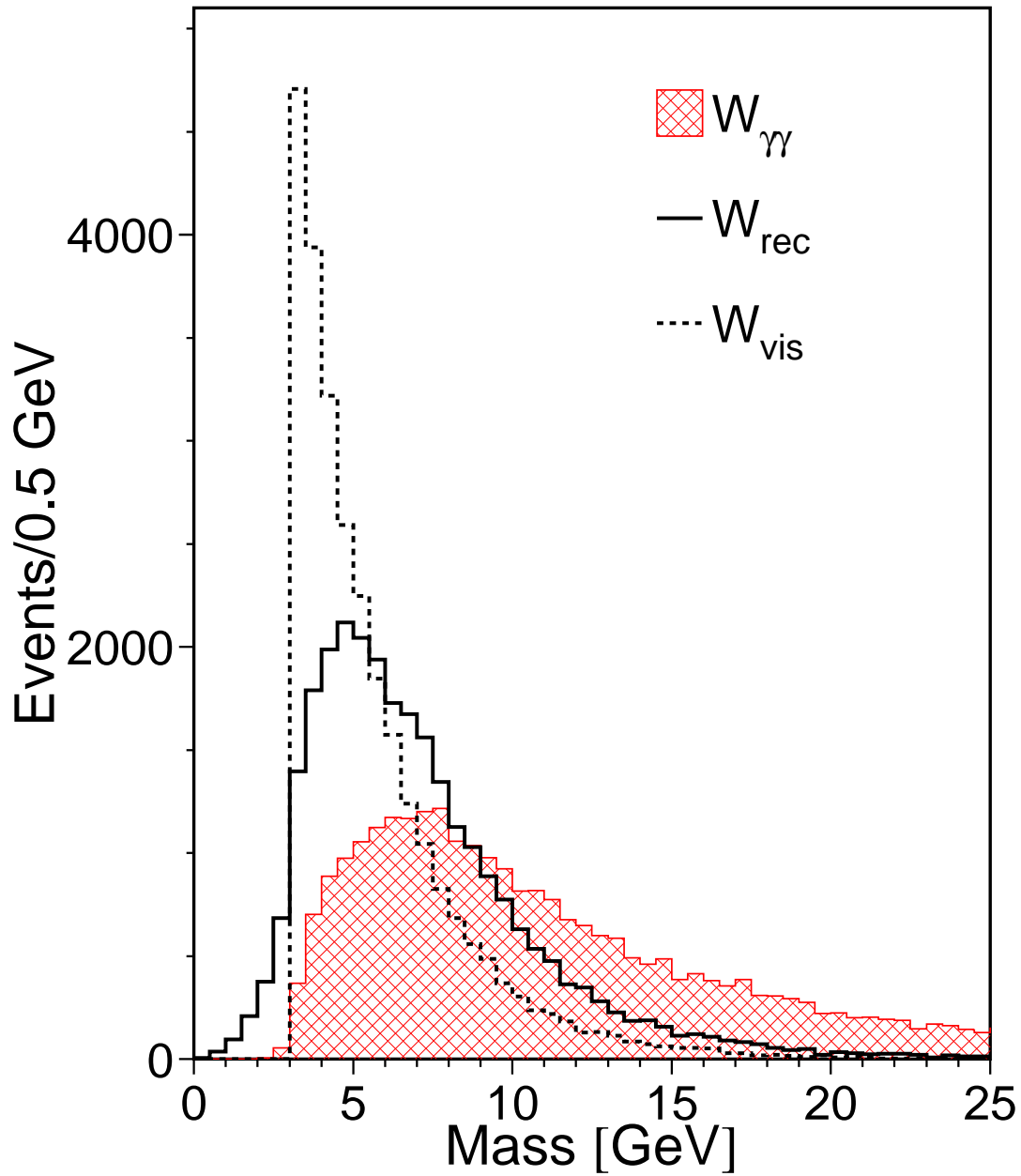


Figure 2: Monte Carlo (PHOJET) comparison of the generated two-photon mass $W_{\gamma\gamma}$ distribution, with the distribution W_{vis} , the mass reconstructed with the measured particles, and W_{rec} , the mass obtained by imposing transverse momentum conservation.

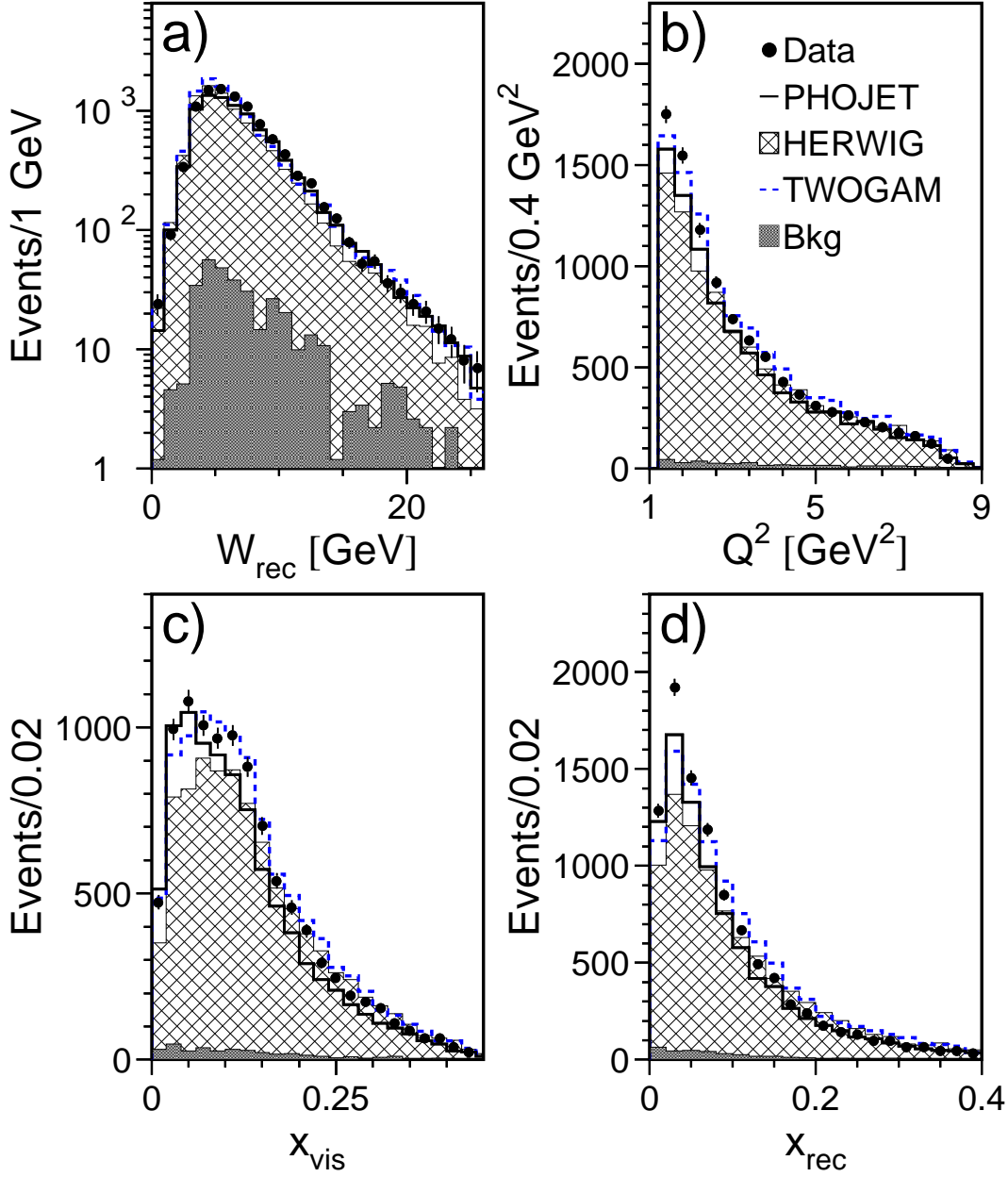


Figure 3: Distribution of a) W_{rec} , b) Q^2 of the tagged electron, c) x_{vis} and d) x_{rec} spectra. The data are compared to the Monte Carlo predictions, normalised to the data luminosity. The backgrounds are from $e^+e^- \rightarrow e^+e^-\tau^+\tau^-$ and $e^+e^- \rightarrow \text{hadrons}$.

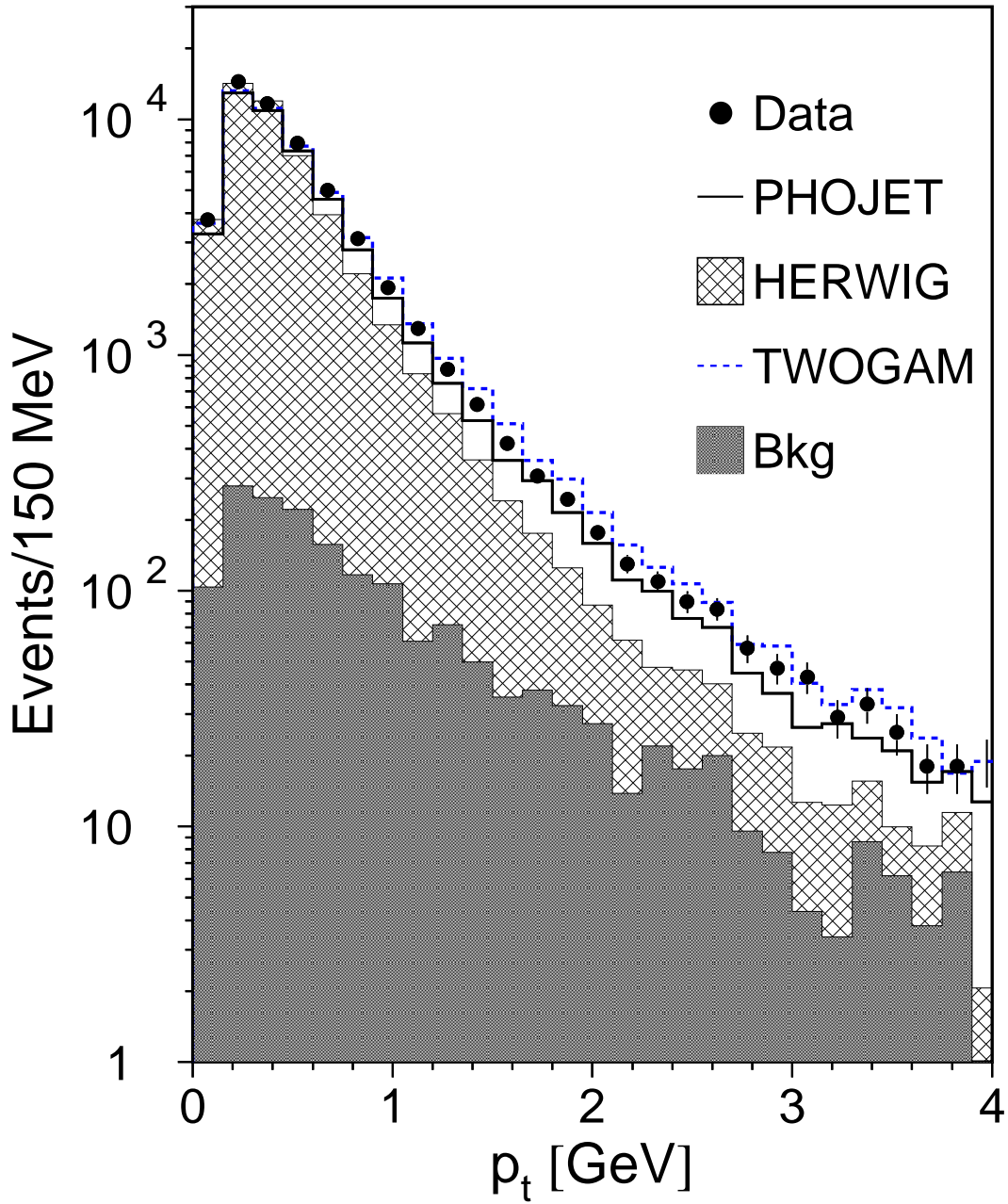


Figure 4: Distribution of the transverse momentum, p_t , of charged particles. The data are compared to the Monte Carlo predictions, normalised to the data luminosity. While PHOJET and TWOGAM reproduce rather well the data, the spectrum of HERWIG is too soft. The backgrounds are from $e^+e^- \rightarrow e^+e^-\tau^+\tau^-$ and $e^+e^- \rightarrow \text{hadrons}$.

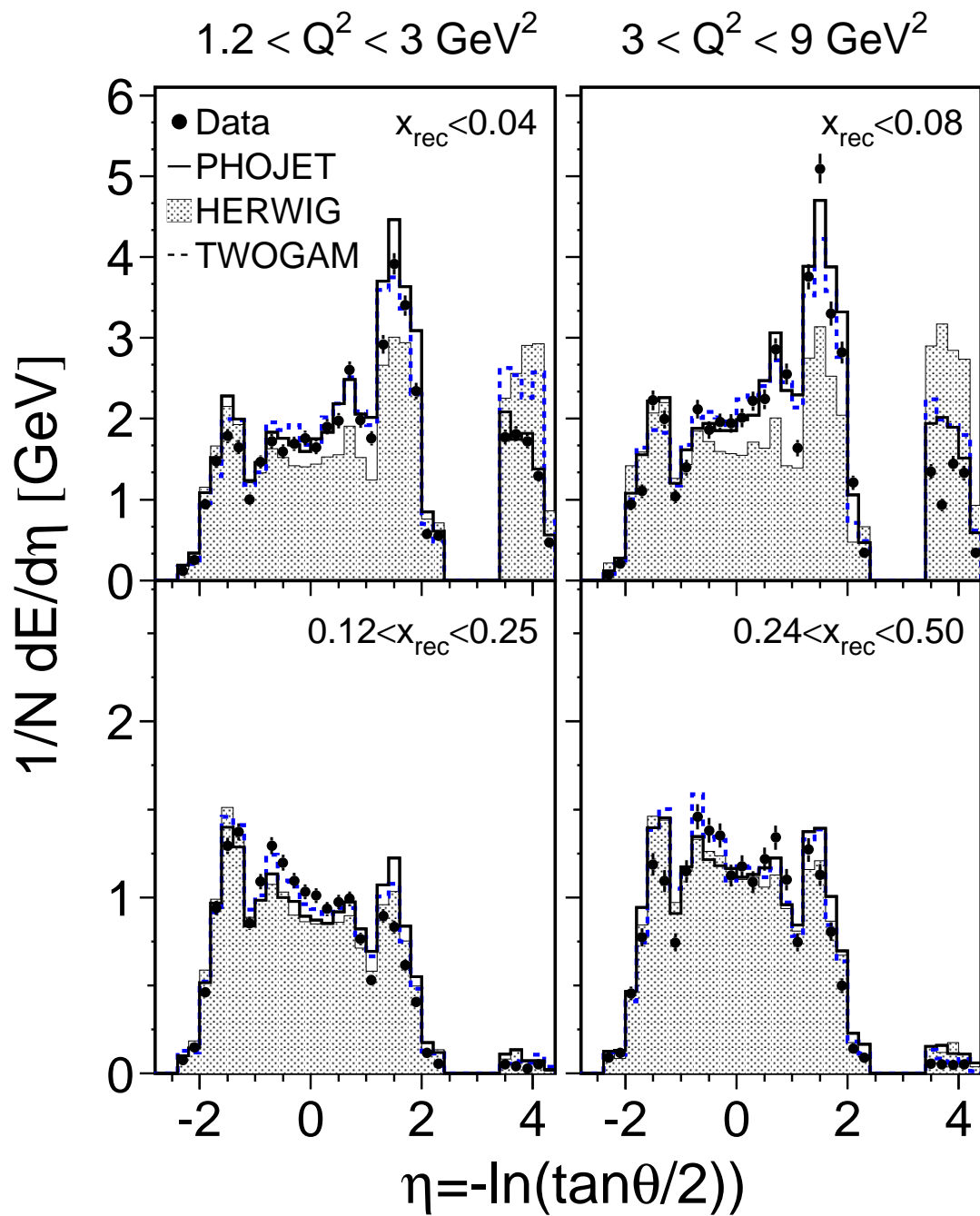


Figure 5: Hadronic energy flow as a function of the pseudorapidity, η , in different Q^2 and x_{rec} bins. The polar angle θ is defined with respect to the tagged electron. The tag direction is always on the negative side.

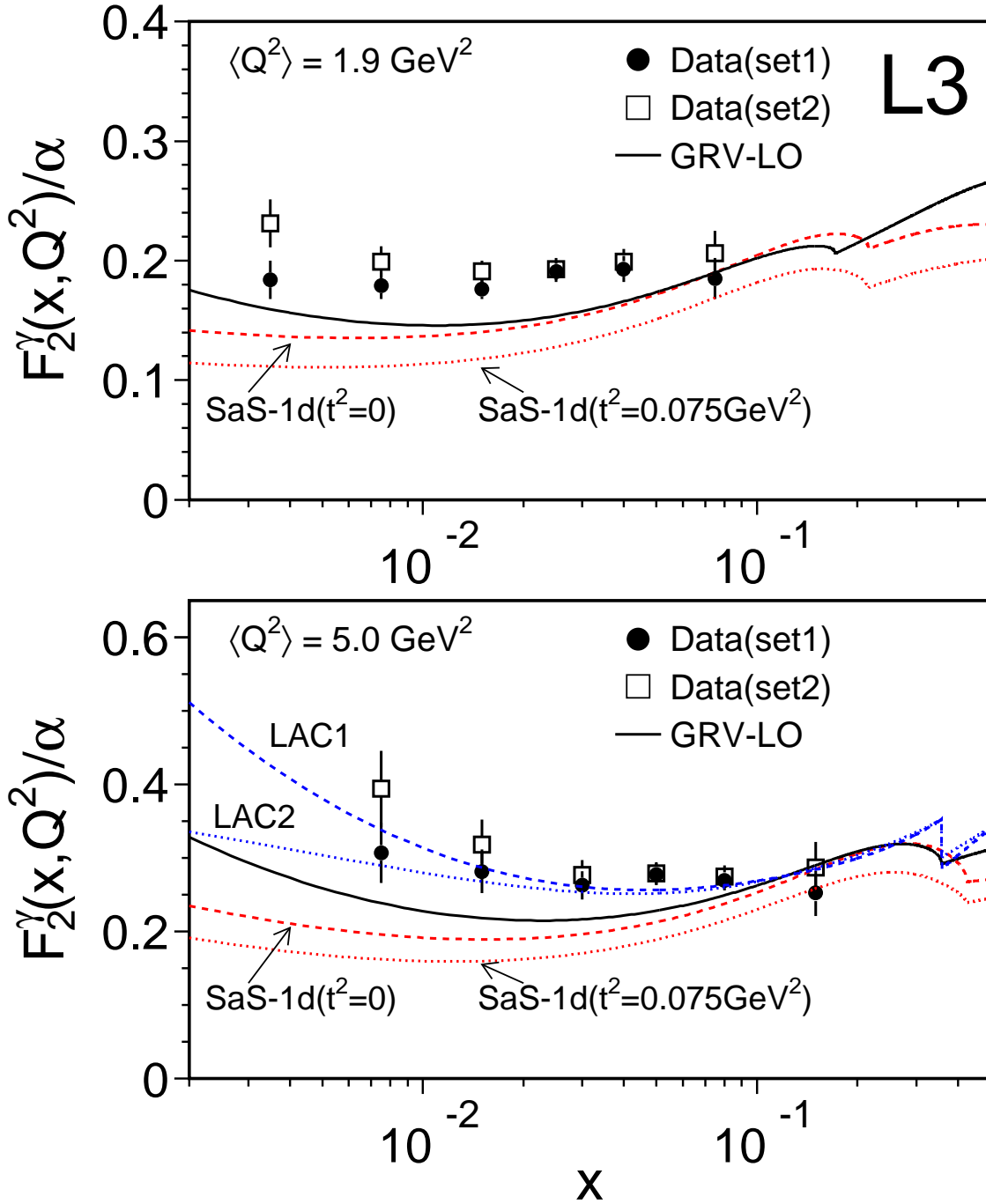


Figure 6: The measured F_2^γ/α at $\langle Q^2 \rangle = 1.9 \text{ GeV}^2$ and $\langle Q^2 \rangle = 5.0 \text{ GeV}^2$ as a function of x . The set1 is unfolded with PHOJET and the set2 unfolded with TWOGAM. The statistical and systematic errors are added in quadrature. The data are compared with the predictions of GRV-LO [5], LAC [7] and SaS-1d [6] at $t^2 = 0$. The prediction of SaS-1d at $t^2 = 0.075 \text{ GeV}^2$ is also indicated. The change of shape of predictions at large x is due to the charm threshold.

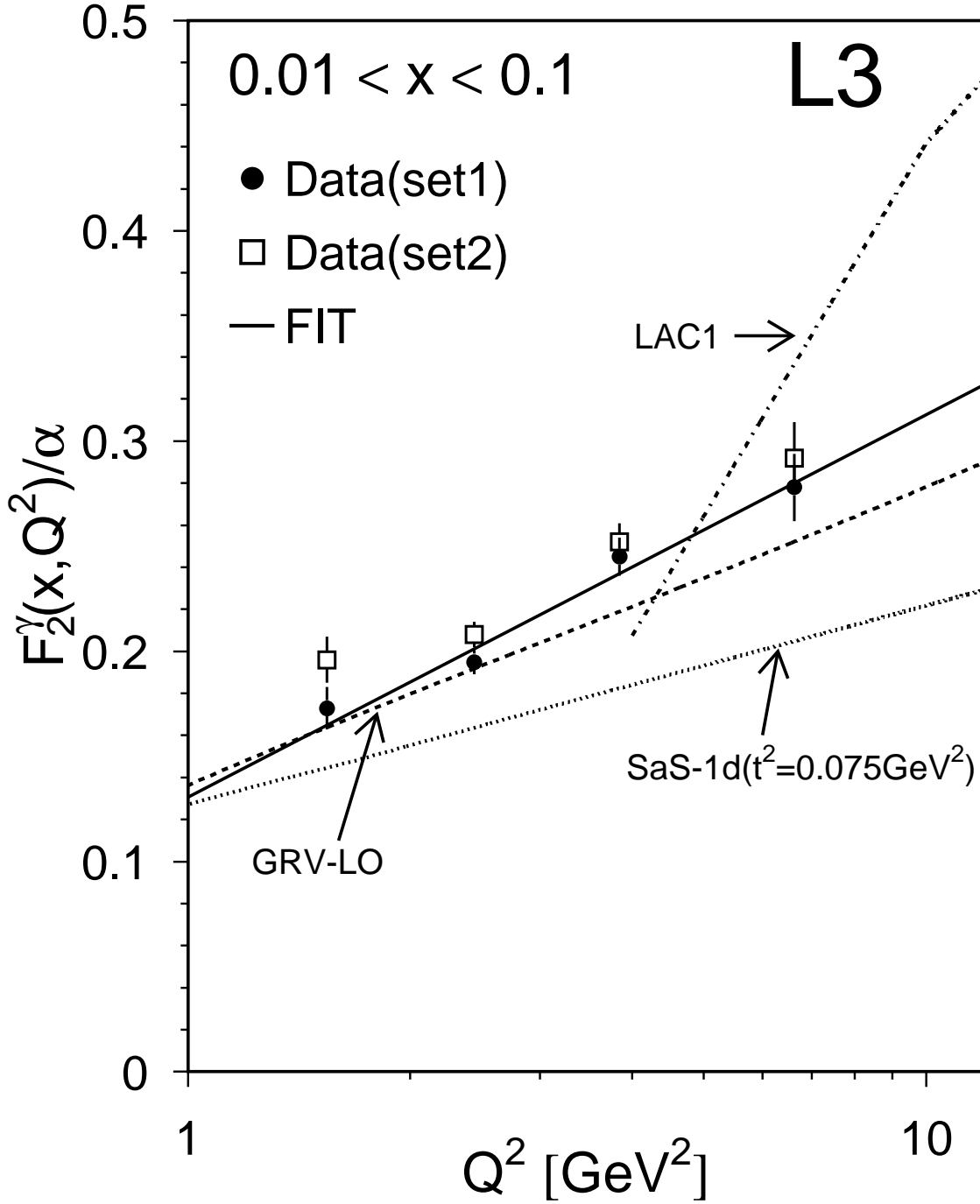


Figure 7: The measured F_2^γ/α as a function of Q^2 compared to the predictions of GRV-LO [5], LAC [7] and SaS-1d [6]. The set1 is unfolded with PHOJET and the set2 unfolded with TWOAM. The solid line is a fit to the data, unfolded with PHOJET, of the function $a+b \ln Q^2$. The statistical and systematic errors are added in quadrature. LAC2 has a similar behaviour as LAC1.